Intraband Auger processes and simple models of the ionization balance in semiconductor quantum-dot lasers

Janet L. Pan*
Research Laboratory of Electronics, Massachusetts Institute of Technology, Cambridge, Massachusetts 02139
(Received 21 October 1993)

The importance of intraband Auger processes in determining the ionization balance in quantum dots is reported. The numerically inexpensive binary-encounter model for a Coulomb collision between identical particles is found to be a good estimator of the intraband Auger rates out of a quantum dot. Intraband and the conventional interband Auger processes differ in that the former involve only intraband transitions whereas the latter always involve a radiationless interband transition. As such, intraband Auger rates do not involve the evaluation of the very small overlap integral of a conduction band with a valence band Bloch wave function and are thus much larger than interband Auger rates, especially for large-band-gap semiconductors like GaAs. Though intraband Auger processes are not strong enough to establish a quasiequilibrium within the entire conduction band at the room-temperature free-carrier concentrations (10^{16} cm^{-3}) and bound energy separations (greater than an LO-phonon energy) commonly assumed in the quantum-dot literature, they are capable of placing almost as many bound carriers in states near the band edge as would be predicted erroneously by a quasiequilibrium Fermi-Dirac distribution. Such large bound state occupations are important for quantum-dot laser design. A sufficient condition for a quasiequilibrium to exist within all of an energy (conduction or valence) band is found to be the existence of many inverse Auger processes faster than interband spontaneous emission, which occurs for total (bound plus free) electron concentrations greater than 5×10^{17} cm^{-3} at room temperature in 100 Å radius GaAs/$Al_{0.3}Ga_{0.7}As$ quantum dots whose centers are separated by 400 Å. The nonlocal thermodynamic equilibrium populations in quantum dots can be understood from a simple model in which states connected by fast Auger or phonon processes are in Saha-Boltzmann equilibrium. All other states have occupation factors which are determined by the ratio of intraband collisional to interband radiative lifetimes, as described by a Fokker-Planck equation modeling diffusion in energy of bound particles.

I. INTRODUCTION

We have recently shown that the assumption of quasiequilibrium within an energy (conduction or valence) band is highly questionable[1,2] over a wide range of temperatures at the typical bound energy separations (greater than an LO phonon energy) and free-carrier concentrations (10^{16} cm^{-3}) commonly assumed[3–6] in the quantum-dot literature. The assumption of quasiequilibrium is indicated by the same quasi-Fermi level (E_{Fc} or E_{Fv}) in the distribution function[7]

$$f_{c,v}(E) = \frac{1}{1+\exp\left([E - E_{Fc,Fv}]/k_BT\right)}, \quad (1)$$

for all the carriers in the same energy band in all the quantum dots and barrier. Our conclusion was based on solution of the population rate equations in which these processes affecting the quantum-dot bound carriers were included: intraband collisional excitation and deexcitation as well as collisional ionization[8] from and three body recombination into all bound states resulting from the Coulomb interaction with incident free particles, interband spontaneous emission, intraband absorption and emission as well as photoionization and radiative recombination resulting from a Planck distribution of photons, ionization from and recombination into weakly bound states resulting from interaction with an equilibrium distribution of LO phonons, and excitation and deexcitation resulting from an equilibrium distribution of small energy acoustic phonons.

The use of a quasiequilibrium (1) for all the carriers within the same energy (conduction or valence) band in all the quantum dots and barrier is justifiable[7,9,10] when intraband (mainly carrier-phonon and carrier-carrier) scattering is much faster than the interband (conduction-to-valence band) radiative emission. In quantum dots having typical bound energy separations greater than an LO phonon energy, intraband relaxation of bound carriers via phonon absorption or emission is insignificant.[11] In a recent paper, a free-carrier concentration in excess of 10^{19} cm^{-3} was found to be required to establish a quasiequilibrium via collisional (de)excitation of bound carriers[2] in a typical example taken from the literature[6] of 100 Å radius GaAs quantum dots whose centers are separated by 400 Å. The typical electron and hole concentrations of 3.125×10^{16} cm^{-3}, which were assumed in the literature,[6] are not large enough to establish a quasiequilibrium via collisional excitation and deexcitation processes within the conduction band of these quantum dots.

0163-1829/94/49(16)/11272(16)/$06.00

The carrier-carrier scattering which helps determine the quantum-dot bound state populations manifests itself as Auger processes as well as collisional (de)excitation. The first purpose of this paper is to distinguish between the conventional interband Auger process shown in Fig. 1 and what we will define to be the intraband Auger processes shown in Fig. 2. The main difference between these two types of Auger processes is that the former always involves a nonradiative interband transition while the latter involves only intraband transitions. We will see in Sec. II that this difference makes intraband much larger than interband Auger rates, especially for large-band-gap semiconductors. We also present the application in both the atomic plasma and quantum-dot literature of the binary-encounter model to the calculation of Auger rates. Discussions are available on interband Auger processes in conventional[7,9,12–15] semiconductors as well as in quantum dots.[16–18] We believe this present work to be the first discussion of intraband Auger processes in quantum dots.

The second purpose of this paper is to include Auger processes in the quantum-dot population rate equations. We find that intraband Auger processes greatly affect the quantum-dot ionization balance, as is borne out in Sec. III. This could have been surmised from the atomic plasmas literature where it has long[19] been known that Auger and dielectronic processes play an important role. Though Auger processes are not strong enough to establish a quasiequilibrium within the conduction band at the room-temperature carrier concentrations and bound energy separations commonly assumed in the literature as discussed in Sec. III B, we do find that intraband Auger processes can place almost as many bound carriers in states near the band edge as would be predicted erroneously by (1). More generally, we discuss in Sec. III B the critical free-carrier concentration above which Auger processes can establish a quasiequilibrium within an energy band.

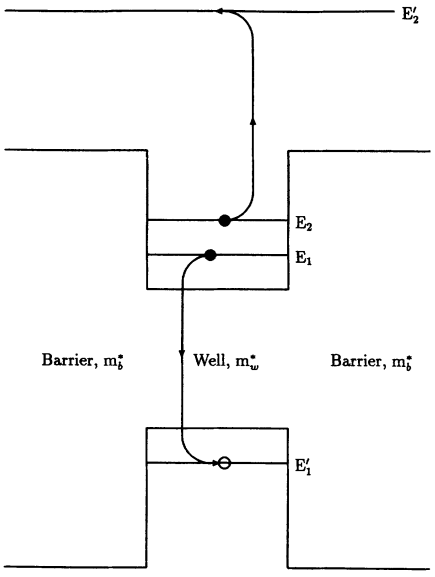

FIG. 1. The energy levels associated with a conventional Auger process. In a conventional or interband Auger process, the energy which ejects the bound particle into a continuum energy state is provided by a nonradiative interband transition. In the CCCV process shown in this figure, the energy released when the initial electron 1 drops into the initial hole state 1′ is absorbed when the initial electron 2 is promoted to the continuum state 2′.

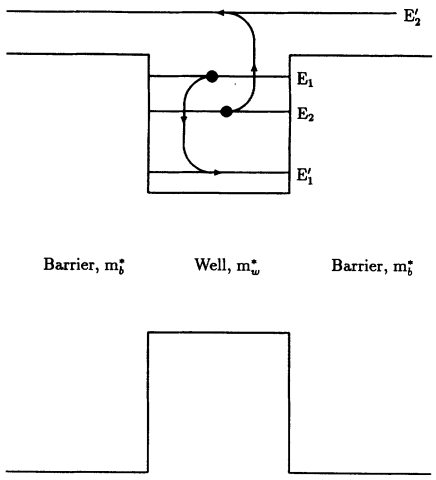

FIG. 2. The energy levels associated with an intraband Auger process. In an intraband Auger process, the energy which ejects the bound particle into a continuum energy state is provided by a nonradiative intraband transition. In the CCCC process shown in this figure, the energy released when the initial electron 1 drops into the lower conduction band state 1′ is absorbed when the initial electron 2 is promoted to the continuum state 2′.

The third purpose of this paper is to give a simple physical understanding of what determines the bound state occupation factors. Knowledge of the nonlocal thermal equilibrium (non-LTE) bound state occupation factors is very helpful in the design of quantum-dot lasers. For example, the population inversion densities and threshold gains and currents are conveniently[20] expressed in terms of the bound state occupations. The model which we present in Sec. III A gives simple, analytical, numerically reliable expressions for the non-LTE bound state occupations useful in quantum-dot laser design. The model clearly indicates the dominant processes establishing the non-LTE bound carrier distribution.

To provide a quantitative example with which to work in this paper, we will use the materials parameters presented in previous[21] work for GaAs quantum dots surrounded by $Al_{0.3}Ga_{0.7}As$ barriers. GaAs has[22] a room-temperature bulk band gap of 1.424 eV, a spin-orbit splitting of 340 meV, an LO phonon energy of 35.34 meV, an index of refraction of 3.3, light hole, heavy hole, and conduction band effective masses at the Γ point of $0.082m_0$, $0.45m_0$, and $0.067m_0$, respectively, and a low frequency dielectric of $12.85\epsilon_0$. Bulk $Al_{0.3}Ga_{0.7}As$ has light hole, heavy hole, and conduction band effective masses at the Γ point of $0.096m_0$, $0.51m_0$, and $0.092m_0$, respectively, a conduction band edge which lies 289.1 meV above that in GaAs, a valence band edge which lies 192.7 meV below

that in GaAs, and a room-temperature[23] low frequency dielectric of $12.01\epsilon_0$. Unless otherwise specified, we will assume room-temperature operation of our quantum dot lasers throughout this paper.

II. INTRABAND AUGER PROCESSES

In an Auger (also known as an autoionizing) process, the energy released by one of the particles originating from an initial two-particle bound state as it drops into a lower energy bound state excites the other particle in the initial two particle state into a higher energy continuum state. When the Auger process involves a radiationless interband transition as shown in Fig. 1, this is the conventional Auger process discussed in the semiconductor literature.[7,9,12–15] When the Auger process involves only intraband transitions as shown in Fig. 2, we define this to be an intraband Auger process to distinguish it from the conventional interband Auger process. We term the intraband Auger process shown in Fig. 2 as a CCCC process by analogy with the common nomenclature of CCCV for the conventional interband Auger process of Fig. 1. The Auger process and its inverse can be indicated by the forward and reverse reactions, respectively, as follows:

$$X(Z,i,j) \rightleftharpoons X(Z+1,k)+e, \tag{2}$$

where the two initial bound electrons in the Auger process are in states i,j in a quantum dot of initial charge Z, and one of the final electrons is in the bound state k, and the other final electron is free.

The interband and intraband Auger processes just defined are analogous to the Auger and super Coster-Kronig transitions, respectively, defined in the literature[24] on atomic inner-shell processes. In an Auger process as defined in the latter, the two initial electrons whose energies will be changed by the Auger process are in a principal subshell different from that containing the initially vacant state which will be filled by the autoionization. In a super Coster-Kronig transition, both of the initial electrons whose energies will be changed by the Auger process are in the same principal subshell as that containing the initially vacant state which will be filled by the autoionization.

A. Calculation of Auger rates

Fermi's golden rule gives the Auger rate as[7,12,25]

$$A_a = \frac{2\pi}{\hbar}\frac{1}{N_{\text{initial}}} \times \sum_{\text{initial states}} \sum_{\text{final states}} |V_{if}|^2\,\delta(E_i - E_f), \tag{3}$$

where N_{initial} is the number of initial states, V_{if} is the matrix element of the Coulomb interaction $V(\mathbf{r}_1-\mathbf{r}_2)=\frac{e^2}{4\pi\epsilon|\mathbf{r}_1-\mathbf{r}_2|}$ between the participating electrons, $\mathbf{r}_1$ and $\mathbf{r}_2$ are the positions of the two electrons, ϵ is the dielectric constant, and E_i and E_f are the total initial and total final energies for the Auger process. The matrix element of $\sum_{i<j}V(\mathbf{r}_i-\mathbf{r}_j)$ between Slater determinantal initial and final states is[26]

$$V_{if} = \int\int d\tau_1 d\tau_2 \{\Phi_1^*(\tau_1)\Phi_2^*(\tau_2) - \Phi_1^*(\tau_2)\Phi_2^*(\tau_1)\} \times V(\mathbf{r}_1-\mathbf{r}_2)\Phi_1'(\tau_1)\Phi_2'(\tau_2), \tag{4}$$

where $i=1,2$, and Φ_i and Φ_i', denote the wave functions of the two initial and final electrons, respectively, where τ represents both spin and spatial coordinates, $\tau=(\sigma,\mathbf{r})$. Included in the rates presented in this paper is an average over all possible initial and a sum over all possible final total (multiparticle) angular momenta.

The multielectron wave functions used in (4) have been discussed before in the literature[18] and are summarized in Appendix A. Single particle wave functions are written[28,29] in $\mathbf{k}\cdot\mathbf{p}$ theory[27] as linear combinations of products of a cell-periodic Bloch part and a slowly varying (over a unit cell) envelope part. The effect of the rotationally symmetric potential formed by the barrier material surrounding the quantum dots is then included in the effective mass approximation in a Schrödinger equation acting[29,28,27] on the envelope part of the wave function. In this rotationally symmetric potential, all wave functions[28,29] are written as total angular momentum eigenstates. The total single particle angular momentum is the vector sum of the electron spin, the microscopic Bloch angular momentum, and the envelope angular momentum. Multiparticle wave functions are chosen to be antisymmetric with respect to all two particle interchanges, as well as to diagonalize the total multiparticle angular momentum.

The direct term in the Auger matrix element (4) is

$$\begin{aligned}
D &= \langle F_1,F_2;F,F_z \mid \frac{1}{|\mathbf{r}_1-\mathbf{r}_2|} \mid F_1',F_2';F',F_z'\rangle \\
&= \sum_{J_2,L_2,J_2',L_2'} C^*_{K_2,J_2,L_2}C_{K_2',J_2',L_2'} \sum_{J_1,L_1,J_1',L_1'} C^*_{K_1,J_1,L_1}C_{K_1',J_1',L_1'} \\
&\times \sum_{\ell=0}^{\infty} R_\ell(1,2,1',2')\delta_{J_1,J_1'}\langle L_1 \,||\, \ell \,||\, L_1'\rangle\,[(2F_1'+1)(2L_1+1)]^{\frac{1}{2}} \\
&\times W(\ell L_1' F_1 J_1; L_1 F_1')\delta_{J_2,J_2'}\langle L_2 \,||\, \ell \,||\, L_2'\rangle \\
&\times [(2F_2'+1)(2L_2+1)]^{\frac{1}{2}}\, W(\ell L_2' F_2 J_2; L_2 F_2')\delta_{F_z,F_z'}\delta_{F,F'}(-1)^{F_1+F_2'-F} \\
&\times [(2F_1+1)(2F_2+1)]^{\frac{1}{2}}\, W(F_1'F_2'F_1F_2;F\ell),
\end{aligned} \tag{5}$$

where J is the quantum number for the vector sum of the single particle spin plus Bloch angular momentum and L is the quantum number for the single particle envelope angular momentum; F_1, F_2, F_1', F_2' are single particle angular momenta and F, F' are multiparticle angular momenta; $C_{K,J_i',L_i'}$ are obtained by diagonalizing the $\mathbf{k}\cdot\mathbf{p}$ Hamiltonian; W(;) is a Racah coefficient;[26] $\langle L||\ell||L'\rangle$ are reduced[30] angular momentum matrix elements; and the Slater integrals $R_\ell(1,2,1',2')$ are integrals of the radial parts of the envelope wave functions, as defined in (A5). (See Appendix A.) The exchange (the second) term in the integral (4) above can be obtained from (5) by replacing the subscripts 1 by 2 and vice versa.

The computation of conventional interband Auger rates involves the evaluation[7,9,12–15] of the very small overlap integral of the mostly s-type Bloch wave function associated with state 1 in Fig. 1 with the mostly p-type Bloch wave function associated with state $1'$ of the same figure. This overlap integral expresses itself in Eq. (5) in the $C_{K,J_i',L_i'}$ coefficients obtained from the $\mathbf{k}\cdot\mathbf{p}$ Hamiltonian: it is largest for the $J=1/2$ term for conduction band states, and it is largest for the $J=3/2$ terms for the light and heavy hole states. For intraband Auger processes, this overlap integral is near unity,[7,9,12] as all Bloch wave functions in intraband scattering have the same symmetry type (mostly either s or p type). This is indicated in Eq. (5) by values of the $C_{K,J_i',L_i'}$ coefficients which are near unity for the same J values for all four states shown in Fig. 2.

The overlap integral of the mostly s- with the mostly p-type Bloch wave functions in the calculation of conventional interband Auger rates is known[7,9,12] to be largest for small-band-gap semiconductors. In fact, the room-temperature, bulk, interband Auger rates are comparable[7,12,18] to interband radiative emission only in semiconductors having band gaps less than about 300 meV. The interband Auger rates in GaAs, with its bulk band gap of 1424 meV, are known[7,12] to be exceedingly small. For this reason, the interband Auger rates in our GaAs quantum dots will not be considered in this work.

The numerical methods used to calculate the intraband Auger rates are the same as those we have previously[18] used for the conventional interband Auger rates. The main difference, of course, is that the four wave functions included in the matrix element (5) are involved only in intraband transitions. Our previous[18] work discussed ways in which we checked our numerical methods.

The numerical example which we discuss in this paper is taken[6] from the literature, that of 100 Å radius GaAs quantum dots whose centers are separated by $d=400$ Å. The materials parameters for GaAs and the $Al_{0.3}Ga_{0.7}As$ barriers were given in the Introduction. The energy levels and symmetries of the bound states in these quantum dots in the effective mass approximation are discussed in Appendix A and elsewhere.[18,21,28,29] They are summarized in Table I.

The intraband Auger lifetimes given in Table II are very short: on the order of tens of picoseconds. They are comparable to the intraband electron-electron scattering rates in the bulk,[9] which is to be expected as the intraband quantum-dot Auger processes become the same as the intraband electron-electron bulk scattering processes in the limit of large quantum-dot radii.

TABLE I. Ten conduction band single particle bound states in a 100 Å radius GaAs quantum dot. The bound state symmetries and energy levels, measured from the GaAs conduction band edge, have been discussed (Ref. 21) elsewhere.

Level number i	Conduction band state	Energy (meV)
0	$1S_{1/2}$	53.7
1	$1P_{1/2}$	105.9
2	$1P_{3/2}$	105.9
3	$1D_{5/2}$	167.4
4	$1D_{3/2}$	167.4
5	$2S_{1/2}$	195.4
6	$1F_{7/2}$	235.6
7	$1F_{5/2}$	235.6
8	$2P_{1/2}$	280.2
9	$2P_{3/2}$	280.2

To have enough energy to autoionize, the energy released by one of the bound particles in the initial two particle state must be enough to raise the energy of the other initially bound electron to a continuum state. Thus the initial two particle state must have at least the energy

$$E_1 + E_2 = E_1' + E_2' \geq E_{\text{min,bound}} + V_B, \tag{6}$$

where $E_{\text{min,bound}}$ is the smallest possible bound energy which E_1' can assume and V_B is the smallest possible continuum energy which E_2' can assume. Thus the initial two particle autoionizing states shown in Table II have energies of at least 362 meV.

B. Comparison with the binary-encounter model

This section presents the application of the binary-encounter model[31–33] to the calculation of Auger rates in both the atomic plasma and quantum-dot literature. When the numerically intensive calculation of the Auger rates by Fermi's golden rule (3) is to be avoided, we find the binary-encounter model to be a good estimator (considering that the bound state degeneracies and symmetries are not accounted for) of these Auger rates in the sense of least-squares fractional error.

The binary-encounter cross sections used here are classical Coulomb cross sections modified to include an exchange term and an interference of the exchange and the direct terms. The main feature of the binary-encounter model is its assumption of an independent pair interaction between the incident and target particles. Another important feature of the binary-encounter model is that it is very easy to use. The binary-encounter model has had semiquantitative[31–33] success in modeling the collisional ionization of electrons from, and to a lesser degree, the collisional excitation in, and the transfer of electrons onto, the target ions in an atomic plasma.

The binary-encounter model is expected to be a good

approximation when the participating electrons come in close proximity during a Coulomb collision. Since the inverse Auger process involves a near Coulomb collision in which the incident particle is captured, the binary-encounter model should be appropriate. In situations where significant contributions to the Coulomb cross section come from distant collisions, such as in collisional ionization processes involving large incident energies and small energy exchanges, the binary-encounter cross section must be augmented[31] to include the effects of distant collisions.

Since the inverse Auger process is a close Coulomb

TABLE II. The CCCC intraband Auger rates in our 100 Å radius GaAs quantum dots surrounded by $Al_{0.3}Ga_{0.7}As$. Included in these rates is an average over all possible initial and a sum over all possible final total (multiparticle) angular momenta. The free-carrier concentration obtained from the rate equations and used to compute the room-temperature inverse Auger rates was 1.04×10^{16} cm^{-3}. The notation is such that 5.40[12] is equal to 5.40×10^{12}.

Initial two particle state		Final bound state			Initial two particle state		Final bound state		
Single particle level number	Single particle level number	single particle level number	Auger rate (1/s)	Inverse Auger rate (1/s)	Single particle level number	Single particle level number	single particle level number	Auger rate (1/s)	Inverse rate (1/s)
1	8	0	5.40[11]	2.98[8]	5	9	1	8.23[11]	2.16[8]
1	9	0	1.54[12]	1.70[9]	5	9	2	5.14[11]	6.75[7]
2	8	0	8.88[11]	9.80[8]	5	9	3	1.24[10]	1.17[7]
2	9	0	7.85[11]	1.73[9]	5	9	4	3.65[11]	5.15[8]
3	5	0	2.57[11]	1.05[9]	6	7	0	5.66[11]	1.40[8]
3	6	0	3.07[11]	1.06[9]	6	7	1	1.65[12]	3.07[9]
3	6	1	3.91[10]	1.02[9]	6	7	2	2.21[12]	2.06[9]
3	6	2	1.30[12]	1.69[10]	6	7	3	5.25[12]	3.49[10]
3	7	0	9.09[11]	2.35[9]	6	7	4	4.87[12]	4.87[10]
3	7	1	5.08[11]	9.91[9]	6	8	0	2.32[11]	3.41[6]
3	7	2	2.43[12]	2.37[10]	6	8	1	6.52[11]	7.24[7]
3	8	0	2.89[11]	4.46[7]	6	8	2	3.50[11]	1.94[7]
3	8	1	6.56[11]	7.64[8]	6	8	3	2.58[12]	1.03[9]
3	8	2	1.75[12]	1.02[9]	6	8	4	3.45[11]	2.05[8]
3	9	0	8.99[10]	2.78[7]	6	8	5	2.55[12]	8.95[9]
3	9	1	1.12[11]	2.60[8]	6	9	0	1.69[11]	4.96[6]
3	9	2	1.53[12]	1.78[9]	6	9	1	1.53[11]	3.39[7]
4	5	0	2.89[11]	7.88[8]	6	9	2	5.33[11]	5.91[7]
4	6	0	9.93[11]	2.29[9]	6	9	3	4.22[12]	3.35[9]
4	6	1	2.10[12]	3.64[10]	6	9	4	1.81[12]	2.16[9]
4	6	2	2.14[12]	1.86[10]	6	9	5	1.47[12]	1.03[10]
4	7	0	2.06[11]	3.56[8]	7	8	0	9.70[10]	1.07[6]
4	7	1	5.48[11]	7.13[9]	7	8	1	2.00[11]	1.67[7]
4	7	2	9.76[11]	6.35[9]	7	8	2	2.07[11]	8.63[6]
4	8	0	6.56[10]	6.75[6]	7	8	3	2.59[12]	7.72[8]
4	8	1	2.76[11]	2.14[8]	7	8	4	1.28[12]	5.72[8]
4	8	2	1.51[12]	5.86[8]	7	8	5	1.86[12]	4.91[9]
4	9	0	3.06[11]	6.30[7]	7	9	0	2.08[11]	4.59[6]
4	9	1	1.68[12]	2.61[9]	7	9	1	2.61[11]	4.34[7]
4	9	2	2.20[12]	1.70[9]	7	9	2	9.09[11]	7.57[7]
5	6	0	4.42[11]	1.72[8]	7	9	3	5.05[12]	3.01[9]
5	6	1	9.79[11]	2.88[9]	7	9	4	2.85[12]	2.54[9]
5	6	2	4.72[11]	6.95[8]	7	9	5	1.39[12]	7.35[9]
5	7	0	3.56[11]	1.04[8]	8	9	0	4.60[11]	6.06[5]
5	7	1	7.16[11]	1.58[9]	8	9	1	7.78[11]	7.73[6]
5	7	2	5.43[11]	5.99[8]	8	9	2	1.02[12]	5.06[6]
5	8	0	9.88[11]	1.72[7]	8	9	3	4.38[10]	1.56[6]
5	8	1	3.79[11]	4.99[7]	8	9	4	6.94[11]	3.70[7]
5	8	2	4.17[10]	2.74[6]	8	9	5	2.43[12]	7.63[8]
5	8	3	1.55[10]	7.27[6]	8	9	6	3.67[10]	1.36[7]
5	8	4	1.58[10]	1.12[7]	8	9	7	6.64[10]	3.30[7]
5	9	0	9.75[11]	3.40[7]					

collision, we follow Vriens[31] in assuming that both the incident and target particles have kinetic energies that are measured relative to the potential in the quantum confined region (from the quantum-dot band edge), as it the relative velocities during the close collision which are most important. The target electrons are assumed to have a velocity distribution appropriate for their bound state. This velocity distribution is assumed to be spherically symmetric, which is a reasonable if one is considering averages over degenerate angular momentum eigenstates.

Vriens[31,32] and Gryzinski[33] have given the differential cross section σ_E for the collision in which an energy E is exchanged between two identical particles interacting via the Coulomb interaction. For the discrete energies involved in a collisional excitation of a bound particle or in the transfer of an electron from an incident atom to a particular state in the target, Vriens[31] and Gryzinski[33] integrate this differential cross section over a range ΔE of the exchanged energy, where $\Delta E = (E_1)_n - (E_1)_{n-1}$ is the energy separation near the energy E_1 of the final state involved in the excitation. The analogous total cross section Q for a collision involving an incident particle and a target electron in a quantum dot is

$$Q \simeq \sigma_E \Delta E = (\pi R^2)\left(\frac{e^2}{4\pi\epsilon_{QD}R}\right)^2\left[\left(\frac{1}{E^2}+\frac{4E_1'}{3E^3}\right)+\left\{\frac{1}{(E_2'-E_1'-E)^2}+\frac{4E_1'}{3(E_2'-E_1'-E)^3}\right\}-\frac{\Phi'}{E(E_2'-E_1'-E)}\right]\frac{\Delta E}{E_2'}, \quad (7)$$

where R is the radius of the quantum dot, ϵ_{QD} is the low frequency dielectric constant in the quantum-dot material, the energies (as shown in Fig. 2 and measured from the quantum-dot band edge) of the two initial particles are E_1' (bound) and E_2' (free) and of the two final bound particles are E_1 and E_2, (7) assumes that the energy exchange $E \equiv E_1 - E_1'$ is defined to be positive, (7) also assumes that $E_2 > E_1'$, and[8,31,32] $\Phi' \simeq 1$. The term in parentheses, the term in curly brackets, and the Φ' term inside the square brackets in (7) are, respectively, the direct, exchange, and interference terms in the Coulomb interaction between identical particles.

Though we have not been able to find in the literature the application of the binary-encounter model to an Auger process, we have observed use of the binary-encounter model in similar problems involving a specified energy exchange in a Coulomb collision: the collisional excitation and electron transfer problems mentioned above. We follow the example of Vriens[31,32] and Gryzinski[33] to write the Coulomb cross section as (7), which we propose to be appropriate for the inverse Auger process considered in this paper. The Auger rate is then obtained from the proposed cross section (7) and detailed balance,

$$A_a = Q v_2' g(E_2') \Delta E, \quad (8)$$

where $v_2' = (2E_2'/m_w)^{\frac{1}{2}}$ is the velocity of the free particle and

$$g(E_2') = \frac{1}{4\pi^2}\left(\frac{2m_b}{\hbar^2}\right)^{\frac{3}{2}}(E_2' - V_B)^{\frac{1}{2}} \quad (9)$$

is the density[34] of states per unit volume per unit energy.

Figure 3 shows the dependence on the final unbound particle energy E_2' (measured from the quantum-dot band edge) of the Auger rates calculated from Fermi's golden rule (3) (circles) and those obtained from the binary-encounter model (8) (squares) for a 200 Å radius GaAs quantum dot surrounded by $Al_{0.3}Ga_{0.7}As$. The numbers in this figure correspond to all Auger processes for which the final bound particle [1′ in (7)] is a $1S_{\frac{1}{2}}$ state at 13.8 meV and for which the energy exchanged in the direct term in (7) is 265.8 meV. The Auger rates calculated from Fermi's golden rule (3) are averaged over all initial autoionizing states which are energy degenerate.

The solid line in Fig. 3 is the best fit curve, which has the form of a fourth order polynomial times the functional form of the binary-encounter Auger rate, to the circles in Fig. 3 in the sense of least-squares fractional[35] error. The agreement between this best fit curve and the binary-encounter numbers (the squares in the figure) is better than 10%. This indicates that the binary-encounter Auger rates are roughly an arithmetic mean of

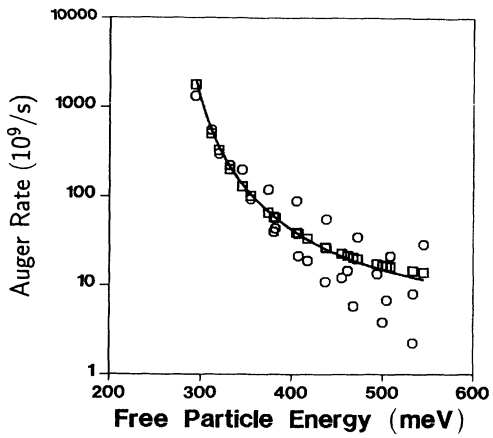

FIG. 3. Comparison of the dependence on the final unbound particle energy (measured from the quantum-dot band edge) of the Auger rates calculated from Fermi's golden rule (3) (circles) and those obtained from the binary-encounter model (8) (squares) for a 200 Å radius GaAs quantum dot surrounded by $Al_{0.3}Ga_{0.7}As$, whose band edge is at 289.1 meV. The solid line is the best fit curve, which has the form of a fourth order polynomial times the functional form of the binary-encounter Auger rate, to the circles in the sense of least squares fractional error. The numbers in this figure correspond to all Auger processes for which the final bound particle [1′ in (7)] is a $1S_{\frac{1}{2}}$ state at 13.8 meV and for which the energy exchanged in the direct term in (7) is 265.8 meV. The Auger rates calculated from Fermi's golden rule (3) are averaged over all initial autoionizing states which are energy degenerate.

the circles in Fig. 3 which have nearly the same abscissa. This makes sense, since in the limit of very large quantum dots, the nearly degenerate states used to calculate the circles in the figure would be precisely energy degenerate, and Fermi's golden rule would then average over all the circles in Fig. 3. Thus, if the numerically intensive calculation of the Auger rates by Fermi's golden rule (3) are not done, then the binary-encounter model appears to be a good estimator (considering that the bound state degeneracies and symmetries are not accounted for) of the Auger rates in the sense of least-squares fractional error.

Figure 4 shows the dependence on the final unbound particle energy E_2' (measured from the quantum-dot band edge) of the Auger rates calculated from Fermi's golden rule (3) (circles) and those obtained from the binary-encounter model (8) (squares and solid line) for a 100 Å radius quantum dot. The numbers in this figure correspond to all Auger processes for which the final bound particle [1′ in (7)] is in one of the states 0 in Table I and for which the energy exchanged in the direct term in (7) is E=226.5 meV. The Auger rates calculated from Fermi's golden rule (3) are taken from Table II after an appropriate average over the initial states which are accidentally degenerate (see Table I).

As with the use of the binary-encounter model in the literature[31,33] for calculating collisional excitation and electron transfer rates in atomic plasmas, the numerical accuracy of the binary-encounter model for estimating Auger rates in quantum dots is limited by the somewhat arbitrary choice of energy range ΔE (because of the discrete nature of the bound energies) for integration

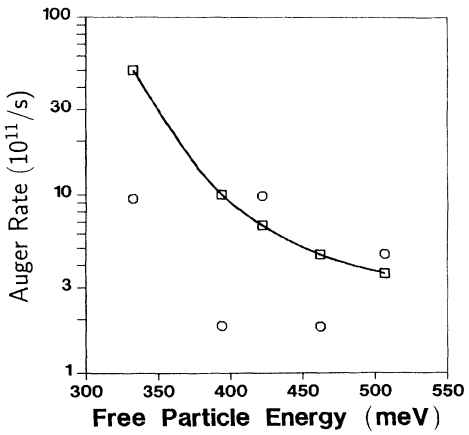

FIG. 4. Comparison of the dependence on the final unbound particle energy (measured from the quantum dot band edge) of the Auger rates calculated from Fermi's golden rule (3) (circles) and those obtained from the binary-encounter model (8) (squares and solid line) for an 100 Å radius GaAs quantum dot surrounded by $Al_{0.3}Ga_{0.7}As$, whose band edge is at 289.1 meV. The numbers in this figure correspond to all Auger processes for which the final bound particle [1′ in (7)] is in one of the states 0 of Table I and for which the energy exchanged in the direct term in (7) is 226.5 meV. The Auger rates calculated from Fermi's golden rule (3) are taken from Table II after an appropriate average over the initial states which are accidentally degenerate (see Table I).

of the differential cross section, and by the way in which bound state degeneracies are not accounted for. These difficulties probably give rise to the discrepancies shown in Figs. 3 and 4 between the Auger rates obtained from Fermi's golden rule and those obtained from the binary-encounter model. No attempt was made to find a best fit curve to the circles in Fig. 4, as too few points are available from this small radius quantum dot.

C. Inverse Auger rates

The inverse Auger rate $n_c\Gamma_c$ in Table II were obtained from the principle of detailed balance,

$$n_c\Gamma_c = A_a \frac{g_a}{g_j}\frac{n_c}{N_C}\exp\left(-\frac{E_{aj}}{k_BT}\right), \tag{10}$$

where the initial autoionizing state a and the final state j (having one fewer electron) have degeneracies of g_a and g_j, respectively, and an energy difference between them of E_{aj}, where n_c is the free electron concentration and the room temperature $N_C=2(2\pi m_{\mathrm{DOS},C}k_BT/h^2)^{3/2}$ is 6.73×10^{17} cm^{-3} in $Al_{0.3}Ga_{0.7}As$. The inverse Auger process, which we have thus defined to be the inverse of that shown in either Fig. 1 or Fig. 2, is known in the literature on atomic processes in plasmas as a radiationless electron capture and is the first step in the two-step dielectronic recombination process discussed by Burgess.[19]

Large inverse Auger rates are required in order for a quasiequilibrium to exist within an energy band, as discussed in Sec. III B. The inverse Auger rates will be large if the Auger rates are large or if the temperature is appropriate. The binary-encounter model of Sec. III B allows one to quickly estimate the largest Auger rates.

The temperature dependence of the inverse Auger rates (10) is shown in Fig. 5, where the E_{aj}=43.3 meV

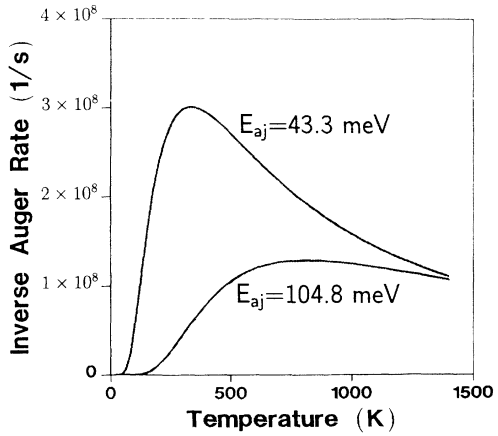

FIG. 5. The temperature dependence of the inverse Auger rates of (10) for $n_c=1.04\times10^{16}$ cm^{-3}. The E_{aj}=43.3 meV and E_{aj}=104.8 meV curves correspond to the first and twelfth entries of Table II. As would be expected from the occupation statistics of the initial free particle, the inverse Auger rates drop exponentially at low temperatures and drop as $T^{-3/2}$ at high temperatures. Thus, the inverse Auger rate is largest at $T=\frac{2}{3}E_{aj}$, where E_{aj} is the initial free particle energy as measured from the continuum (barrier) band edge. Large inverse Auger rates are required in order for a quasiequilibrium to exist within an energy band, as discussed in Sec. III B.

and E_{aj}=104.8 meV curves correspond to the first and twelfth entries of Table II, respectively, for n_c=1.04×10^{16} cm^{-3}. As would be expected from the occupation statistics of the initial free particle, the inverse Auger rates drop exponentially at low temperatures and drop as $T^{-3/2}$ at high temperatures. Thus the inverse Auger rate is largest at $T = \frac{2}{3}E_{aj}$, where E_{aj} is the initial free particle energy as measured from the continuum (barrier) band edge.

III. IONIZATION BALANCE

This section discusses the effect of intraband Auger processes on the ionization balance in quantum dots. The population rate equations are solved for the example of the preceding section of 100 Å radius GaAs quantum dots whose centers are separated by d=400 Å. Since typical bound *hole* states are separated by only a few[21] meV in our 100 Å radius GaAs quantum dots, we will assume that fast phonon processes maintain the valence band in a quasiequilibrium (1). Thus, in this section, we are only interested in the rate equations describing the populations in quantum-dot *conduction* band states.

The time rate of change of the concentration of quantum dot ions is[2,36]

$$\frac{d\,N(I)}{dt} = \sum_{J\neq I}[A_a(I,J) + C(I,J) + A_r(I,J) + P(I,J)]N(J) - N(I)\sum_{J\neq I}[\,A_a(J,I) + C(J,I) + A_r(J,I) + P(J,I)\,], \quad (11)$$

where I, J are particular ion configurations $(Z,\{i\})$ and $A_a(I,J)N(J)$, $C(I,J)N(J)$, $A_r(I,J)N(J)$, and $P(I,J)N(J)$ are the fluxes contributing to a decrease in $N(J)$ and an increase in $N(I)$ resulting from all bound-bound and bound-free transitions caused by, respectively, Auger, collisional, radiative, and phonon processes. The set of equations (11) differs from the ones we have previously[2] solved in that we have included on the right hand side of (11) those fluxes which result from intraband Auger processes. A detailed discussion of the rate coefficients for the bound-bound and bound-free collisional, radiative, and phonon processes in quantum dots is given[2,8] in the literature.

Equations (11) are solved in the steady state subject to the boundary conditions that the total concentration of carriers in each band and the total concentration of ions are fixed. The total concentration of ions is

$$\sum_{\{I\}} N(\{I\}) = \sum_{(Z,\{j\})} N(Z,\{j\}) = N_{\rm ion} = d^{-3} \quad (12)$$

because the spacing d between quantum-dot centers is fixed by the fabrication procedure. The total concentration $n_{c,\rm tot}$ of conduction band electrons is

$$n_{c,\rm tot} = n_c + \sum_{\text{bound } i} n_i, \quad (13)$$

the sum of the concentration of the free electrons n_c and of the electrons in all bound states i. In (13), n_i is the number of electrons in the bound state i, averaged over all quantum-dot ion configurations,

$$n_i = \frac{\sum_{\{I\}} n_{i,I} N(\{I\})}{\sum_{\{I\}} N(\{I\})}, \quad (14)$$

where $n_{i,I}$ is the known number of electrons in the single particle state i in the particular quantum-dot ion configuration I.

The total concentration of electrons and holes was chosen to be the same as that discussed before in the literature,[1,2,6] $n_{c,\rm tot}$=3.125×10^{16} cm^{-3}. This choice of

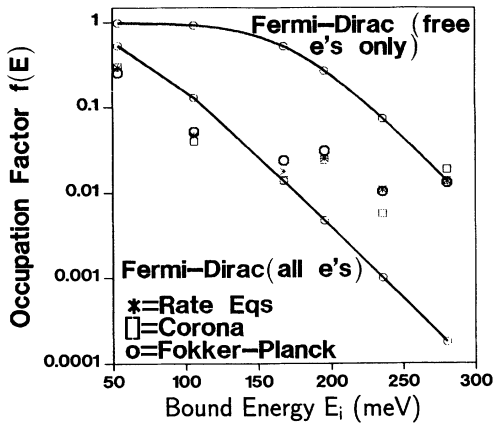

FIG. 6. Comparison of the predictions of various models for the bound state occupation probabilities in the conduction band of our 100 Å radius GaAs quantum dots whose centers are separated by 400 Å. The occupation probabilities predicted by the rate equations (labeled as stars) are seen to be in good agreement with the predictions of the Corona (squares) and Fokker-Planck (boldfaced circles) models. Both the Corona and Fokker-Planck models assume that the states differing in ionization which are connected by fast Auger or LO phonon processes are in Saha-Boltzmann equilibrium. In the corona model, all other electronic states are assumed to have zero occupation. These states which are not affected by fast Auger or LO phonon processes are assumed in the Fokker-Planck model to have nonzero occupations determined by a Fokker-Planck equation modeling diffusion of electrons in energy. In spite of predicting occupation probabilities vastly different from the quasiequilibrium distribution function (1) commonly assumed in the literature for *all* conduction band electrons [Fermi-Dirac (all e's) with E_{Fc}=56.7 meV], the rate equations do predict the occupation of the bound states at 53.7 meV to be almost the same as that obtained by assuming a quasiequilibrium for *all* conduction band electrons. Electrons in quasiequilibrium with the *free* electrons would have the distribution labeled Fermi-Dirac (free e's only). The electrons in the bound states at 280.2 meV, which is well within an LO phonon energy of the $Al_{0.3}Ga_{0.7}As$ band edge at 289.1 meV, are seen to be in quasiequilibrium with the free electrons and all other bound electrons have occupations which are less than that predicted by the upper solid curve in this figure. The steady state total concentration of conduction band electrons was assumed to be 3.125×10^{16} cm^{-3}.

total carrier concentration is optimal for quantum-dot laser studies: a much smaller total carrier concentration would result in very small bound state occupations and a much larger concentration would result in sizeable occupations for many bound states which do not contribute to the intended laser line.

At a total concentration of $n_{c,\mathrm{tot}}=3.125\times10^{16}$ cm^{-3} conduction band electrons, three ionization stages were included in our model: nonionized (with $Z=0$ and 2 bound conduction band electrons per quantum dot), singly ionized (with $Z=1$ and 1 bound conduction band electron per quantum dot), and doubly ionized (with $Z=2$ and no bound conduction band electrons per quantum dot).

The quantum-dot bound state occupation factor plotted in Fig. 6 is defined to be

$$f_c(E_i)=\frac{n_i}{g_i N_{\mathrm{ion}}}, \tag{15}$$

where n_i is the average number of electrons in the bound state i (14).

The bound state occupation probabilities for our 100 Å radius GaAs quantum dots predicted by the rate equations in (11) are shown in Fig. 6 as stars. The rate equation occupation probabilities differ vastly from the quasiequilibrium distribution function (1) commonly assumed in the literature for *all* conduction band electrons [Fermi-Dirac (all e's) with $E_{Fc}=56.7$ meV]. In spite of this, the rate equations do predict the occupation of the bound states at 53.7 meV to be almost the same as that obtained by erroneously assuming a quasiequilibrium for *all* conduction band electrons. These rate equation occupation probabilities are seen to be in good agreement with the predictions of the corona and Fokker-Planck models, which are discussed below.

The solution of the rate equations (11) predicts a free electron concentration of $n_c=1.04\times10^{16}$ cm^{-3} out of a possible $n_{c,\mathrm{tot}}=3.125\times10^{16}$ cm^{-3} total conduction band electrons. The *free* electrons are assumed to be in quasiequilibrium and thus can be described by a quasi-Fermi level of 170 meV above the GaAs bulk band edge. Electrons in quasiequilibrium with the *free* electrons would have the distribution labeled "Fermi-Dirac (free e's only)." The electrons in the bound states at 280.2 meV, which is well within an LO phonon energy of the $Al_{0.3}Ga_{0.7}As$ band edge at 289.1 meV, are seen to be in quasiequilibrium with the free electrons. All other bound electrons have occupations which are less than that predicted by the Fermi-Dirac (free e's only) curve in this figure.

A. Simple models

Before discussing some simple models which help us to understand the numerical answers given by the rate equations we first show that the Fermi-Dirac (all e's) model which assumes (1) with the same quasi-Fermi level E_{Fc} for all conduction band electrons could not possibly be correct at room temperature and the total carrier concentration assumed above. If one were to assume, by way of contradiction, that (1) *is* valid for all 3.125×10^{16} cm^{-3} conduction band electrons, then the Fermi level for *all* electrons is $E_{Fc}=56.7$ meV and only[1,2] 8.5×10^{13} cm^{-3} electrons remain free. Using the numbers presented in this paper, the inverse Auger lifetimes at such a small free carrier concentration are on the order of microseconds and are much longer than the interband spontaneous emission lifetimes. Thus the assumption of (1) for all the conduction band electrons at room temperature and $n_{c,\mathrm{tot}}=3.125\times10^{16}$ cm^{-3} yields intraband Auger rates (as well as collisional[2] ionization and excitation rates) which are too weak to be consistent with the assumption of (1).

With the exception of our previous[2] work, we have not been able to find any discussion of rate equations modeling the ionization balance in quantum-dot lasers. With a view towards numerically checking the rate equation solutions as well as developing physical understanding, we now propose two models which may be of use in the design of quantum-dot lasers. Both of these models are conceptually the same as the statistical theories[37] commonly used in the literature on atomic processes in plasmas to describe the excited-level and ionization-state populations. Such statistical equilibrium (steady state) approaches reduce the full set of rate equations (11) to a much smaller set by observing that states connected by a fast (e.g., Auger) process have steady state populations which are related. The smaller set of rate equations are then solved for the level populations which change more slowly in time.

1. Corona model

To emphasize a similarity between quantum dots and atomic ions, we have borrowed the name of our first model, the corona model, from the atomic plasma[38] literature. In both the corona model of atomic plasmas and the corona model which we are about to propose for quantum dots, the excitation and ionization balance problems may be separated. In atomic ions of increasing nuclear charge, the excitation processes which are studied occur at a rate much faster than that of the ionization. Consequently, once the ionization balance is known, the atomic ion states with the same ionization can be assumed to have a Saha-Boltzmann distribution. In the literature on the corona model in high temperature plasmas, it is well known[39] that a crucial role in determining the populations of the variously charged ions is played by those autoionization processes which result in placing ions in their various excited states. Such autoionization processes are analogous to the intraband Auger processes discussed here, since the latter place electrons in the various conduction band excited states.

In quantum dots, the fast and slow processes are reversed. This paper has already shown Auger rates to be on the order of tens of picoseconds and inverse Auger rates to be on the order of tens of nanoseconds. From previous work,[2] intraband collisional excitation, intraband spontaneous emission, and interband spontaneous emission lifetimes are on the order of 100 ns, 10 μs, and 10 ns, respectively. In the corona model of quantum dots, processes (ionization and recombination through Auger and LO phonon processes) faster than the inter-

band spontaneous emission determine the distribution of the population among the different ionization sequences, and slow processes (intraband collisional and radiative processes) determine the distribution of the population among states with the same ionization.

Figure 7 shows as stars the relative populations of the two particle states $\frac{N(Z=0,E)g(Z=0,E=516\text{ meV})}{N(Z=0,E=516\text{ meV})g(Z=0,E)}$ obtained from the rate equation solution. The two particle states with energies satisfying (6) are seen to be in Saha-Boltzmann equilibrium with each other because they are connected by fast Auger processes to singly ionized quantum dots. The two particle states with energies less than what is required in (6) are seen to have populations much less than that predicted by a Saha-Boltzmann equilibrium. We will see in Sec. III A 2 that the two particle states which are energetically incapable of autoionizing are populated by slow intraband collisional and radiative

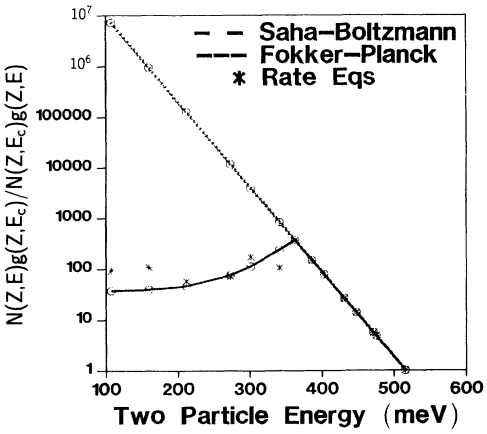

FIG. 7. The relative occupation of the two particle states $\frac{N(Z=0,E)g(Z=0,E=516\text{ meV})}{N(Z=0,E=516\text{ meV})g(Z=0,E)}$. The relative occupations predicted by the rate equations (labeled as stars) are seen to be in good agreement with the predictions of the Fokker-Planck model (solid curve). The Fokker-Planck model takes all electronic states connected by fast Auger or phonon processes to be in Saha-Boltzmann equilibrium and all other electronic states are assumed to have nonzero occupations determined by a Fokker-Planck equation modeling diffusion of electrons in energy. For our 100 Å radius GaAs quantum dots surrounded by $Al_{0.3}Ga_{0.7}As$, the two particle states which participate in Auger processes have energies exceeding 362 meV. As indicated in (18), those two particle states with energies just less than 362 meV are populated by the diffusion of carriers from higher energy states. The characteristic energy of this diffusion in energy is determined by the ratio of typical interband radiative rates to typical collisional (de)excitation rates. The populations of two particle states with energies much less than 362 meV are determined by the ratio of the three body recombination influx to the interband radiative outgoing flux. The corona model of Fig. 6 also assumes that electronic states connected by fast Auger or phonon processes are in Saha-Boltzmann equilibrium, but all other electronic states are assumed to have zero occupation. The dashed curve indicates the relative occupations that would be predicted if all two particle states were in Saha-Boltzmann equilibrium. The numbers in this figure were used to compute those in Fig. 6.

processes. These ideas are now used to propose a corona model for quantum dots.

The deviation of the ion populations from Saha-Boltzmann equilibrium is defined through the coefficients $b(Z=1,i)$ in

$$N(Z=1,i) = N(Z+1)\frac{g(Z,i)}{g(Z+1)}\frac{n_c}{N_C}\exp\left(\frac{U_i}{k_BT}\right) \times b(Z=1,i), \tag{16}$$

where i is a bound state in the conduction band. For a Saha-Boltzmann equilibrium, all the coefficients $b(Z=1,i)$ are equal to unity.

In the corona model of quantum-dot ionization balance, the ratio of the ion populations are taken to be (16) with

$$b(Z,i) = 1 \tag{17}$$

for all states connected by a fast Auger or a LO phonon process. (This is only a rough approximation, as the inverse Auger processes are comparable to and not greater than the interband radiative processes for our numbers.) In the corona model, all other states are assumed to have zero population because the intraband collisional and radiative processes populating them are much slower than the interband spontaneous emission. The concentrations of each ion and of the free carriers are then found by requiring that the total concentrations of ions and free carriers are fixed by (12) and (13).

Figure 6 shows good agreement between the results of the rate equations and the corona model. This is a corroboration of the main features of the corona model: most of the lower energy single particle bound states in Fig. 6 are populated by electrons in singly ionized quantum dots and the higher energy single particle states are populated by electrons in unionized quantum dots. By lower energy single particle bound states, we mean those with energies less than half of (6). The setting to zero of the populations of those two particle bound states which do not participate in fast processes (those in Fig. 7 with energies less than 362 meV) in the corona model is a good rough approximation because the occupation of the low energy single particle bound states in Fig. 6 comes mainly from singly ionized quantum dots rather than from unionized quantum dots with total energy less than 362 meV.

The rate equations predict the occupation of the bound states at 53.7 meV in Fig. 6 to be almost the same as that obtained by assuming a quasiequilibrium for *all* conduction band electrons. The reason is that the singly ionized quantum dots are in Saha-Boltzmann equilibrium with each other and with the unionized quantum dots which have energies satisfying (6), and the Saha-Boltzmann distribution (17) predicts quantum dots having a single electron at 53.7 meV to have the highest occupation. The quantum dot conduction band still cannot be described by (1) because many of the two-particle states with energies less than that required by (1) have populations much smaller than in Saha-Boltzmann equilibrium.

2. Fokker-Planck model

The Fokker-Planck model of this subsection is an extension of the corona model of the preceding section. As in the corona model, the populations of states which are connected by processes much faster (mainly Auger and LO phonon) than the interband spontaneous emission are modeled to be in Saha-Boltzmann equilibrium. Unlike the corona model, the Fokker-Planck model prescribes finite populations for states which are affected only by processes slower than the interband spontaneous emission. Good numerical agreement is found between the rate equations and Fokker-Planck solutions.

The most important processes determining a bound state population in our simple models were found by determining the dominant fluxes on the right hand side of the rate equations (11). The populations of bound states not affected by a fast Auger or LO phonon process were found to be determined by the size of the interband radiative emission relative to intraband collisional excitation, ionization, and their inverse processes. The recombination of a conduction band electron with a valence band hole with the simultaneous emission of a photon constitutes an interband radiative process. A collisional excitation or ionization process denotes the transition of a bound particle to a higher energy bound or continuum state, respectively, with the transition energy provided by an incident free particle. As in our previous work,[2] our simple models make use of the fact that intraband radiative processes are much weaker than intraband collisional processes because of the relatively small size of the typical transition energies involved.

We will assume that groups of degenerate or nearly degenerate states are separated by more than an LO phonon energy so that the interaction of bound particles with phonons is not important. Moreover, we assume as in our previous work[2] that the energy density of bound states, the collisional (de)excitation rates, and the interband spontaneous emission rates do not vary much for the different bound states. We also invoke the fact[8] that the collisional ionization rate $n_c q_E^{cc}$ for a quasiequilibrium distribution of projectiles has roughly the exponential dependence $\exp(-U_i/k_BT)$ on bound state ionization potential U_i.

The standard form (B4) of the steady state Fokker-Planck equation was first used by Pitaevskii[40] to describe the diffusion in energy of bound particles via collisional excitation and deexcitation processes. In a recent[2] paper, we have added to (B4) the fluxes of bound particles resulting from the faster interband spontaneous emission and the slower intraband collisional ionization and three body recombination processes. Thus states which are not affected by a fast Auger or LO phonon process have populations which are determined by the modified Fokker-Planck equation (B8) of Appendix B. Appendix B gives a version of the Fokker-Planck model which differs from our previous[2] discussion in that simple analytical expressions for the deviation from Saha-Boltzmann equilibrium are given. These analytical expressions easily show the regimes where the different physical processes are dominant.

Appendix B shows that the deviation from Saha-Boltzmann equilibrium $b(Z,E)$ of states which are not affected by fast Auger or LO phonon processes can be found from a Sturm-Liouville equation obtained from the Fokker-Planck equation,

$$b(Z,E) = \left(1 - \frac{n_c q_E^{cc}|_{E_c}}{A_{cv}}\right) \times \exp\left[\left(\frac{E-E_c}{k_BT}\right) \times \left(\frac{1}{2} + \frac{1}{2}\left\{1 + \frac{4A_{cv}(k_BT)^2}{B}\right\}^{\frac{1}{2}}\right)\right] + \frac{n_c q_E^{cc}}{A_{cv}}, \tag{18}$$

where A_{cv} and $B/(k_BT)^2$ are, respectively, the interband spontaneous emission and collisional (de)excitation rates and E_c is the energy of the lowest two particle state which is in Saha-Boltzmann equilibrium with higher energy states. We have imposed the boundary conditions

$$b(Z,E_c) = 1 \text{ and } b(Z, E \to E_{\min}) = \frac{n_c q_E^{cc}}{A_{cv}}, \tag{19}$$

because we require that two particle states with energies greater than or equal to E_c are in Saha-Boltzmann equilibrium and that very small energy two particle states have populations determined by the ratio of the three body recombination influx to the interband radiative outgoing flux. This second boundary condition was found[1,2] to be exhibited by the rate equation solution. Based on the numerics of our previous paper,[2] we have chosen the parameters in equation (18) to be $A_{cv} \sim B$ and $\frac{n_c q_E^{cc}|_{E_c}}{A_{cv}} \simeq 0.1$.

Figure 7 shows good agreement between the rate equation solution and the Fokker-Planck model for the occupations of the two particle states. The errors in Fokker-Planck model come from variations with respect to the different bound states of the energy density of bound states, and interband radiative and collisional transition rates. Figure 6 shows the rate equation solution to be in better (in the sense of mean squared error in occupation probability) agreement with the Fokker-Planck model than with the corona model. This is a result of the more careful modeling of the populations of the two particle states which are not affected by fast LO phonon or Auger processes.

Our analytical solution (18) gives a good physical description of how the two particle states are populated. The states with energies greater than E_c are in Saha-Boltzmann equilibrium because of fast Auger or LO phonon processes. Those two particle states with energies just less than E_c are populated by the diffusion of bound carriers from higher energy states, as indicated by the exponential term in (18). Equation (18) shows the characteristic energy of this diffusion in energy to be determined by the ratio of typical interband radiative rates to typical collisional (de)excitation rates: a large ratio indicates that electrons do not diffuse very far in energy before combining with a valence band hole. Diffusion re-

sulting from collisional (de)excitation does not affect the populations of two particle states with energies much less than E_c. The population of these latter states is shown in Eq. (18) to be determined by the ratio of the three body recombination influx to the interband radiative outgoing flux.

B. Critical free carrier concentration for LTE

As mentioned in the Introduction, the use of a quasiequilibrium (1) for all the carriers within the same energy (conduction or valence) band in all the quantum dots and barrier is highly questionable[1,2] over a wide range of temperatures at the typical bound energy separations (greater than an LO phonon energy) and free carrier concentrations (10^{16} cm^{-3}) commonly assumed in the quantum-dot literature. The reason is that the intraband relaxation of bound carriers via phonons[11] and collisional[2] (de)excitation is slower than the interband spontaneous emission in such quantum dots. How do Auger processes affect this discussion?

When the total number of conduction band electrons is very large, many of the quantum-dot ionization stages have sizeable occupations, and many are connected by large fluxes resulting from Auger and inverse Auger processes. A sufficient condition for Auger and inverse Auger processes to establish (1) for all the carriers within the same energy band is that the free carrier concentration be large enough in order for the slowest inverse Auger process to be faster than the interband spontaneous emission. The minimum free carrier concentration $n_{c,\mathrm{crit}}$ to satisfy this criterion is

$$n_{c,\mathrm{crit}}\Gamma_c = 10A_{cv}. \tag{20}$$

The slowest inverse Auger rate given in Table II is $(1.66\ \mu\mathrm{s})^{-1}$, and Eq. (20) yields a $n_{c,\mathrm{crit}} \sim 10^{19}$ cm^{-3} for this Γ_c. This latter value of $n_{c,\mathrm{crit}}$ is probably pessimistically large, as the states connected by a very slow inverse Auger rate may also be connected to other states by much faster inverse Auger rates.

A more realistic value of $n_{c,\mathrm{crit}} \sim 10^{17}$ cm^{-3} comes from using the median value of Γ_c given in Table II. This free carrier concentration corresponds to a E_{Fc}=241.1 meV (48 meV below the $Al_{0.3}Ga_{0.7}As$ conduction band edge). Using (13), the total conduction band population is then

$$\begin{aligned} n_{c,\mathrm{tot,crit}} &= n_{c,\mathrm{crit}} \\ &\quad + N_{\mathrm{ion}} \sum_{\text{bound } i} \frac{g_i}{1+\exp\left([E_i - E_{Fc}]/k_BT\right)} \\ &\sim 5.37\times 10^{17}\mathrm{cm}^{-3}, \end{aligned} \tag{21}$$

where we have explicitly used (1) and E_{Fc}=241.1 meV for all quantum-dot and barrier conduction band electrons. Thus, for a quasiequilibrium within the conduction band, Eq. (21) requires a much larger total (bound plus free) conduction band population than the 3.125×10^{16} cm^{-3} assumed in the example of this paper.

It is most likely that practical quantum-dot lasers will not be operated with free-carrier concentration greater than $n_{c,\mathrm{crit}}$ for reasons of efficiency. At the free-carrier concentration of $n_{c,\mathrm{crit}}$, the quasiequilibrium carrier distribution shows too many bound states to have large occupations. For example, at $n_{c,\mathrm{crit}}$ in our 100 Å radius quantum dots, the Fermi energy of E_{Fc}=241.1 meV shows that 34 of the bound states in Table I (including the angular momentum degeneracies) have occupations greater than one-half. Thus the injected current supplies a population inversion over a wide spectral region, of which much is at frequencies away from the intended laser line. This is undesirable.

IV. CONCLUSIONS

We have reported the importance of intraband Auger processes in determining the ionization balance in quantum dots. Though intraband Auger processes are not strong enough to establish a quasiequilibrium within the entire conduction band at the room-temperature free-carrier concentrations (10^{16} cm^{-3}) and bound energy separations (greater than an LO phonon energy) commonly assumed in the quantum-dot literature, they are capable of placing almost as many bound carriers in states near the band edge as would be erroneously predicted by a quasiequilibrium Fermi-Dirac distribution. Such large bound state occupations are important for quantum-dot laser design.

The binary-encounter model for a Coulomb collision between identical particles is found to be a good estimator (considering that the bound state degeneracies and symmetries are not accounted for) of intraband Auger rates and is thus useful when calculation of the latter by the numerically intensive Fermi golden rule is to be avoided. Intraband and the conventional interband Auger processes differ in that the former involve only intraband transitions whereas the latter always involve a radiationless interband transition. Intraband Auger rates do not involve the evaluation of the very small overlap integral of a conduction band with a valence band Bloch wave function. Thus intraband Auger rates are much larger than interband Auger rates for large-band-gap semiconductors like GaAs.

A sufficient condition for a quasiequilibrium to exist within all of an energy (conduction or valence) band is found to be the existence of inverse Auger processes much faster than interband spontaneous emission, which occurs for total (bound plus free) electron concentrations greater than 5×10^{17} cm^{-3} at room temperature in 100 Å radius $GaAs/Al_{0.3}Ga_{0.7}As$ quantum dots. A particular inverse Auger process is strongest when the temperature k_BT is on the order of the free particle energy. Quasiequilibrium within all of an energy band is probably not desirable for practical quantum-dot lasers, as many bound states would then have occupations close to unity and the population inversion would be wasted in spectral regions of no interest.

The non-LTE quantum-dot bound state occupations can be understood from a simple model in which states connected by fast Auger or phonon processes are in Saha-Boltzmann equilibrium. All other states have occupation factors which are determined by the ratio of intraband collisional to interband radiative lifetimes, as described by a Fokker-Planck equation modeling diffusion of bound

particles in energy. A simple model for the non-LTE occupation factors is useful for obtaining quantities important in quantum-dot laser design, such as population inversion densities, threshold gains, and currents.

APPENDIX A: THE MULTIPARTICLE STATES USED IN CALCULATING THE AUGER MATRIX ELEMENTS

In the $\mathbf{k}\cdot\mathbf{p}$ energy band theory with total angular momentum eigenstates as a basis, the energy eigenstates[28] in a quantum sphere must also be eigenstates of the total angular momentum

$$\mathbf{F} = \mathbf{J} + \mathbf{L} = \mathbf{S} + \mathbf{L}_B + \mathbf{L}, \tag{A1}$$

where $\mathbf{S}$, $\mathbf{L}_B$, and $\mathbf{L}$ are the spin, Bloch, and envelope angular momenta quantum numbers, respectively. Thus the energy eigenstates $\Phi'_{i'}(\tau)$ are

$$\begin{aligned}\Phi'_{i'}(\tau) &= \langle \tau \mid F'_i, F'_{iz}\rangle \\ &= \sum_{J'_i, L'_i} C_{K,J'_i,L'_i} f_{L'_i}(Kr)\langle \sigma_{J'_i}, \Omega \mid J'_i, L'_i; F'_i, F'_{iz}\rangle,\end{aligned} \tag{A2}$$

where $f_{L_i}(Kr)$ is the radial part of the envelope function for each different angular momentum term, K is the magnitude of the bound carrier wave vector, and

$$C_{K,J'_i,L'_i} = \langle J'_i, L'_i; F'_i, F'_{iz}; K \mid F'_i, F'_{iz}; K\rangle \tag{A3}$$

are determined by diagonalizing the $\mathbf{k}\cdot\mathbf{p}$ Hamiltonian in the $\mid F'_i, F'_{iz}; J'_i, L'_i\rangle$ basis.

There are two requirements on the form of the multiparticle states: antisymmetry with respect to the interchange of any two particles and all multiparticle states must be eigenstates of total multiparticle angular momentum. In atomic physics, these two requirements are met through the use of[41,42] recoupling coefficients and[41,43] coefficients of fractional parentage. When there are no more than two particles in each single particle energy level, as in the case computed in this paper, the formalism of the coefficients of fractional parentage is not needed. Antisymmetry with respect to two particle interchanges is already ensured by the use of a Slater determinant in (4). For our two particle states, we use a linear combination of Slater determinants to ensure that the initial and final two particle states are eigenstates of total angular momentum,

$$\begin{aligned}&\mid F_1, F_2; F, F_z\rangle \\ &\quad= \sum_{F_{1z},(F_{2z}=F_z-F_{1z})} \mid F_1, F_{1z}\rangle \mid F_2, F_{2z}\rangle \\ &\qquad\times\langle F_1, F_{1z}; F_2, F_{2z} \mid F_1, F_2; F, F_z\rangle.\end{aligned} \tag{A4}$$

The Slater integrals in (5) are

$$\begin{aligned}R_\ell(1,2,1',2') = &\int_0^\infty r_2^2 dr_2 \int_0^\infty r_1^2 dr_1 f^*_{L_2} \\ &\times (K_2 r_2) f_{L'_2}(K'_2 r_2) \\ &\times \frac{4\pi}{2\ell+1}\frac{r_<^\ell}{r_>^{\ell+1}} f^*_{L_1}(K_1 r_1) \\ &\times f_{L'_1}(K'_1 r_1),\end{aligned} \tag{A5}$$

where R is the radius of the quantum dot.

APPENDIX B: FOKKER-PLANCK DESCRIPTION OF THE DIFFUSION IN ENERGY OF BOUND CARRIERS

The use of a Fokker-Planck equation to describe diffusion in energy was first discussed by Pitaevskii,[40] and is appropriate to model collisional-radiative[44] recombination in plasmas. The purpose of this appendix is to review the diffusion in energy of bound carriers in a quantum dot as described by a Fokker-Planck equation. The use of a Fokker-Planck equation is appropriate when there is one process [collisional (de)excitation in this paper] which dominates the random walk among the bound energy states. We will be modifying the Fokker-Planck equation to account for strong interband radiative emission and three body recombination (the inverse of collisional ionization). Assuming that the energy density of states and the collisional deexcitation rates do not vary much for the different bound states, which is appropriate for our quantum dot, we can obtain analytical expressions for the deviations from Saha-Boltzmann equilibrium.

The use of a Fokker-Planck equation to model the random walk of electrons among the bound energy states can be understood from expressions for the steady state flux of particles into and out of the different bound energies. The steady state solution of the rate equations must satisfy

$$\sum_{j\neq i}[X_{ji}N(Z,j) - X_{ij}N(Z,i)] = 0, \tag{B1}$$

where X_{ji} is the sum of the rates for all processes in which a carrier goes from state j to state i. It has the general solution[40,44]

$$\begin{aligned}\sum_{\ell=1}\sum_{i=0}\{\, &X_{(j+\ell),(j-i)}N[Z,(j+\ell)] \\ &- X_{(j-i),(j+\ell)}N[Z,(j-i)]\,\} = -J,\end{aligned} \tag{B2}$$

where $-J$ is the downward flux of carriers past state $(j+\frac{1}{2})$.

When only terms with small ℓ and i contribute significantly in (B2), and when X_{ij} and X_{ji} are related by detailed balance,

$$X_{ji} = \frac{g_i}{g_j} X_{ij} \exp\left(\frac{E_{ji}}{k_B T}\right), \tag{B3}$$

then the difference in Eq. (B2) can be approximated by a derivative in the limit of quasicontinuous bound states.

The total downward flux (B2) can be written as a Fokker-Planck equation[2,40,44] for a steady-state problem,

$$-J = B(E)\left(\frac{dF}{dE} - \frac{F}{\rho}\frac{d\rho}{dE} + \frac{F}{k_BT}\right), \tag{B4}$$

where the energy density of states is ($\Delta E_j = E_{j+\frac{1}{2}} - E_{j-\frac{1}{2}}$)

$$\rho(Z, E_j) = g(Z, E_j)/\Delta E_j, \tag{B5}$$

where the energy density of the population distribution is

$$\begin{aligned} F(Z, E_j) &= \frac{N(Z,j)}{\Delta E_j} \\ &= N(Z+1)\frac{\rho(Z,E_j)}{g(Z+1)}\frac{n_c}{N_C}\exp\left(-\frac{E_j}{k_BT}\right) \\ &\quad \times b(Z, E_j), \end{aligned} \tag{B6}$$

where $b(Z, E_j)$ is the deviation from Saha-Boltzmann equilibrium, and where the diffusion coefficient in the Fokker-Planck equation is

$$B(E_j) = \frac{1}{2}\sum_{E_{ji}} X(E_{ji})E_{ji}^2. \tag{B7}$$

Equation (B4) is valid whenever one process and its inverse completely dominate the random walk in energy and must be modified if other processes are involved. For quantum dots, the dominant process, whose rate is X_{ji}, maintaining the random walk among conduction band bound states is collisional (de)excitation. However, an electron, whose collisional deexcitation is to be modeled, may begin its random walk, not with a collisional deexcitation from the continuum, but with a three body recombination into a bound state. Further, the random walk of any specific electron is terminated by an interband radiative transition.

Thus the total downward flux past the quantum dot bound energy E in (B4) must be augmented to include[2] interband radiative emission, collisional ionization, and three body recombination,

$$\begin{aligned} -J = B(E)&\left(\frac{dF}{dE} - \frac{F}{\rho}\frac{d\rho}{dE} + \frac{F}{k_BT}\right) \\ &+ \int_E^{E_{\max}} dE'' F(E'') A_{cv}(E'') \\ &+ \int_{E_{\min}}^{E} dE'' \frac{F(E'')}{b(E'')}\left[1 - b(E'')\right] n_c q_{E''}^{cc}, \end{aligned} \tag{B8}$$

where $E_{\min}$ and $E_{\max}$ are, respectively, the lowest and highest energies in the ionization sequence, $A_{cv}(E)$ is the sum of all rates originating at the conduction band energy E and terminating in the valence band, $n_c q_{E''}^{cc}$ is the collisional ionization rate, and the three body recombination rate coefficient has been related to the collisional ionization rate coefficient by detailed balance. We have assumed that Auger and phonon processes do not significantly affect the states whose populations are to be found from (B8).

The first three terms in the parentheses in (B8) are the downward flux resulting from collisional excitation and deexcitation only. The first integral in (B8) is the interband radiative flux originating from states with energy greater than E. The second integral in (B8) is the three body recombination flux terminating in states with energy less than or equal to E.

As in our previous[2] work, we now assume that

$$B(E), \rho(Z, E) \sim \text{constant in } E, \tag{B9}$$

since the typical degeneracies, bound energy separations, and dominant collisional rate coefficients do not vary much for each of the different bound states. Thus

$$\frac{d}{dE}\left(\frac{F(Z,E)}{b(Z,E)}\right) \simeq -\frac{1}{k_BT}\frac{F(Z,E)}{b(Z,E)} \tag{B10}$$

and we can differentiate (B8) with respect to E to obtain

$$\frac{d^2b}{dE^2} - \frac{1}{k_BT}\frac{db}{dE} - \left[A_{cv}(E) + n_c q_E^{cc}\right]\frac{b(Z,E)}{B(E)} = -\frac{n_c q_E^{cc}}{B(E)}. \tag{B11}$$

Often, it is only necessary to solve (B11) for $b(Z, E)$ for those quantum dot ions which contain strongly bound electrons, since quantum dot ions which contain weakly bound electrons are in Saha-Boltzmann equilibrium and are already accounted for in the corona model. The collisional ionization rate coefficients are usually very small[8] for strongly bound electrons. Thus we can often assume

$$n_c q_E^{cc} \ll B(E) \tag{B12}$$

in (B11). If we further assume that $A_{cv}(E)$ is roughly a constant, which we have found to be true[2] for our 100 Å radius GaAs quantum dots, then (B11) has the homogeneous solutions

$$\begin{aligned} b(Z,E) = \exp&\left[\left(\frac{E - E_c}{k_BT}\right)\right. \\ &\left.\times\left(\frac{1}{2} + \frac{1}{2}\left\{1 + \frac{4A_{cv}(k_BT)^2}{B}\right\}^{\frac{1}{2}}\right)\right] \end{aligned} \tag{B13}$$

or

$$\begin{aligned} b(Z,E) = \exp&\left[\left(\frac{E - E_c}{k_BT}\right)\right. \\ &\left.\times\left(\frac{1}{2} - \frac{1}{2}\left\{1 + \frac{4A_{cv}(k_BT)^2}{B}\right\}^{\frac{1}{2}}\right)\right], \end{aligned}$$

where E_c is the ion energy above which quantum dot ions of charge Z are in Saha-Boltzmann equilibrium.

When A_{cv} is roughly independent of energy, and when the collisional ionization rate coefficients have the following typical[8] exponential dependence on energy:

$$n_c q_E^{cc} \sim \exp\left(\frac{E - E_c}{k_BT}\right), \tag{B14}$$

both the homogeneous and particular solutions of the differential equation (B11) can be found. With the substitution,

$$w(E) = k_B T \exp\left(\frac{E - E_c}{k_B T}\right), \tag{B15}$$

the homogeneous part of Eq. (B11) can be written explicitly as a Sturm-Liouville equation, with $n_c q_E^{cc}|_{E_c}$ equal to the collisional ionization rate evaluated at the energy E_c,

$$\frac{d^2 b}{dw^2} - \left[A_{cv}\left(\frac{k_B T}{w}\right)^2 + n_c q_E^{cc}|_{E_c}\left(\frac{k_B T}{w}\right)\right]\frac{b(w)}{B} = 0, \tag{B16}$$

whose solutions are modified Bessel functions[45]

$$\text{homogeneous} \quad b(w) \sim w^{\frac{1}{2}} I_\nu\left(\lambda w^{\frac{1}{2}}\right) \tag{B17}$$

or

$$\text{homogeneous} \quad b(w) \sim w^{\frac{1}{2}} K_\nu\left(\lambda w^{\frac{1}{2}}\right),$$

where

$$\lambda^2 = 4\frac{n_c q_E^{cc}|_{E_c} k_B T}{B}, \quad \nu^2 = 1 + 4\frac{A_{cv}(k_B T)^2}{B}. \tag{B18}$$

When the arguments of the Bessel functions in (B17) are small, (B17) reduces to (B13).

The particular solution of (B11) is easily found when the collisional ionization rates are known to have the exponential dependence of (B14) and when the interband radiative lifetime is either much larger or much shorter than the collisional ionization lifetimes involved in Eq. (B8). A particular solution of (B11) is

$$\text{particular} \quad b(Z,E) = \begin{cases} \frac{n_c q_E^{cc}}{A_{cv}} & \text{for } A_{cv} \gg n_c q_E^{cc} \\ 1 & \text{for } A_{cv} \ll n_c q_E^{cc}, \end{cases} \tag{B19}$$

as can be verified by direct substitution. When collisional ionization lifetimes are much shorter than interband radiative lifetimes, we expect that collisional processes are fast enough to establish a Saha-Boltzmann equilibrium among ions of charge Z, as indicated by the lower equation in (B19).

The complete solution for $b(Z,E)$ is a linear combination of the homogeneous and particular solutions. For our quantum dots, the numbers in our previous paper[2] show that the collisional ionization rates for the states which do not participate in Auger or LO phonon processes are much smaller than typical collisional excitation and interband radiative rates. For our quantum dots, we can thus write the complete solution for $b(Z,E)$ as

$$b(Z,E) = \left(1 - \frac{n_c q_E^{cc}|_{E_c}}{A_{cv}}\right) \times \exp\left[\left(\frac{E - E_c}{k_B T}\right) \times \left(\frac{1}{2} + \frac{1}{2}\left\{1 + \frac{4A_{cv}(k_B T)^2}{B}\right\}^{\frac{1}{2}}\right)\right] + \frac{n_c q_E^{cc}}{A_{cv}}, \tag{B20}$$

where we have imposed the boundary conditions

$$b(Z,E_c) = 1, \quad b(Z, E \to E_{\min}) = \frac{n_c q_E^{cc}}{A_{cv}}. \tag{B21}$$

ACKNOWLEDGMENTS

The author is greatly indebted to P. L. Hagelstein for many fruitful discussions and much encouragement. Rockwell International is gratefully acknowledged for financial support.

*Present address: 350 Memorial Drive, Cambridge, MA 02139-4304.

[1] J. L. Pan (unpublished).
[2] J. L. Pan (unpublished).
[3] M. Asada, Y. Miyamoto, and Y. Suematsu, IEEE J. Quantum Electron. **QE-22**, 1915 (1986).
[4] Y. Arakawa and H. Sakaki, Appl. Phys. Lett. **40**, 939 (1982).
[5] Y. Miyamoto, Y. Miyake, M. Asada, and Y. Suematsu, IEEE J. Quantum Electron. **QE-25**, 2001 (1989).
[6] K. J. Vahala, IEEE J. Quantum Electron. **QE-24**, 523 (1988).
[7] G. P. Agrawal and N. K. Dutta, *Long Wavelength Semiconductor Lasers* (Van Nostrand Reinhold, New York, 1986).
[8] J. L. Pan, Phys. Rev. B **49**, 2536 (1994).
[9] B. K. Ridley, *Quantum Processes in Semiconductors* (Oxford University Press, New York, 1988).
[10] A. Yariv, *Quantum Electronics* (Wiley, New York, 1975).
[11] H. Sakaki, Jpn. J. Appl. Phys. **28,** L314 (1989).
[12] A. Haug, *Theoretical Solid State Physics* (Pergamon, New York, 1972).
[13] A. Haug, D. Kerkhoff, and W. Lochmann, Phys. Stat. Solidi B **89,** 357 (1978).
[14] M. G. Burt, J. Phys. C **14,** 3269 (1981).
[15] M. G. Burt, S. Brand, C. Smith, and R. A. Abram, J. Phys. C **17**, 6385 (1984).
[16] A. I. Ekimov and Al. L. Efros, Acta Physica Pol. A **79,** 5 (1991).
[17] R. A. Abram, R. W. Kelsall, and R. I. Taylor, J. Phys. Chem. Solids **49,** 607 (1988).
[18] J. L. Pan, Phys. Rev. B **46,** 3977 (1992).
[19] A. Burgess, Astro. J. **139,** 776 (1964).
[20] J. L. Pan (unpublished).
[21] J. L. Pan, Phys. Rev. B **46,** 4009 (1992).
[22] *Handbook of Chemistry and Physics,* edited by R. C. Weast (CRC, Boca Raton, FL 1989).
[23] *Numerical Data and Functional Relationships in Science and Technology,* Landolt-Börnstein, New Series (Springer-Verlag, New York, 1982).
[24] E. J. McGuire, in *Atomic Inner-Shell Processes,* edited by B. Crasemann (Academic, New York, 1975), p. 293.
[25] A. R. Beattie and P. T. Landsberg, Proc. R. Soc. London Ser. A **219**, 16 (1959).
[26] M. Tinkham, *Group Theory and Quantum Mechanics* (McGraw-Hill, New York, 1964).
[27] E. O. Kane, J. Phys. Chem. Solids **1,** 249 (1957).
[28] P. C. Sercel and K. J. Vahala, Phys. Rev. B **42,** 3690 (1990).
[29] J.-B. Xia, Phys. Rev. B **40,** 8500 (1989).

[30]M. Rotenberg, R. Bivins, N. Metropolis, and J. K. Wooten, Jr., *The 3-j and 6-j Symbols* (Technology Press, Cambridge, MA, 1959).
[31]L. Vriens, in *Case Studies in Atomic Collision Physics I,* edited by E. W. McDaniel and M. R. C. McDowell (Wiley, New York, 1969), p. 335.
[32]L. Vriens, Proc. Phys. Soc. **89,** 13 (1966).
[33]M. Gryzinski, Phys. Rev. **138,** A336 (1965).
[34]This definition of the density of states does not have an extra factor of 2 for the spin degeneracy because the spin of the final particle must be the same as the initial.
[35]The least-squares *fractional* error criterion is used rather than a simple least-squares error criterion because the former does a better job fitting points having small magnitude. This criterion is applied to the magnitude of the circles in Fig. 3 rather than to the logarithm of the magnitude so that the fitted curve is a measure of the arithmetic rather than the geometric mean of the circles which have nearly the same abscissa.
[36]A. Burgess and H. P. Summers, Mon. Not. R. Astron. Soc. **174,** 345 (1976).
[37]V. L. Jacobs and J. Davis, Phys. Rev. A **18** 697 (1978).
[38]H. R. Griem, *Plasma Spectroscopy* (McGraw-Hill, New York, 1964).
[39]V. L. Jacobs, J. Davis, P. C. Kepple, and M. Blaha, Astrophys. J. **211**, 605 (1977).
[40]L. P. Pitaevskii, Zh. Eksp. Teor. Fiz. **42**, 1326 (1962) [Sov. Phys. JETP **15,** 919 (1962)].
[41]U. Fano, Phys. Rev. **140,** A67 (1965).
[42]P. G. Burke, Comput. Phys. Commun. **1,** 241 (1970).
[43]G. Racah, Phys. Rev. **63,** 367 (1943).
[44]G. J. Pert, J. Phys. B **23,** 619 (1990).
[45]M. Abramowitz and I. A. Stegun, *Handbook of Mathematical Functions with Formulas, Graphs, and Mathematical Tables* (National Bureau of Standards, Washington, DC, 1964).